Heliyon 7 (2021) e07969

Contents lists available at ScienceDirect

Heliyon

journal homepage: www.cell.com/heliyon

Research article

# Synthesis, spectral characterization, lethal dose ($LD_{50}$) and acute toxicity studies of 1,4-Bis(imidazolylazo)benzene (BIAB)

Hussein Ali Kadhim Kyhoiesh [a,*], Mohammed K. Al-Hussainawy [a], Azal Shakir Waheeb [b], Khalid J. Al-Adilee [c]

[a] Ministry of Education, Directorate of Education Al-Muthanna, Al-Samawah, AL-Muthanna, Iraq
[b] Department of Chemistry, College of Science, University of Al-Muthanna, Al-Samawah, Iraq
[c] Department of Chemistry, College of Education, University of Al-Qadisiyah, Diwaniya 1753, Iraq

## HIGHLIGHTS

- BIAB has been prepared, spectrally characterized and bioactivity assays (antimicrobial, anti-oxidative and $LD_{50}$).
- (BIAB) was tested in-vitro for *Staphylococcus aureus*, *Escherichia coli*, Aspergillus Niger and *Candida albicans*.
- (BIAB) have been shown to have acute toxicity lethal doses ($LD_{50}$) 1020.23 mg/kg.
- The half-maximal inhibitory concentration ($IC_{50}$) is 224.17 μg/ml.

## ARTICLE INFO

*Keywords:*
Imidazole
FE-SEM
XRD
Antibacterial
$LD_{50}$
$IC_{50}$

## ABSTRACT

The preparation and spectral identification of new heterocyclic azo ligand 1,4-Bis(imidazolylazo)benzene (BIAB) was prepared by reacting a diazonium chloride salt solution of 1,4-diaminobenzene with imidazole in alkaline ethanolic solution. Differing spectral techniques have been used to study the structure of the azo dye ligand (BIAB) such as Elemental analysis (C.H.N), $^{1}$H-NMR, Mass spectrum, UV-Vis, FT-IR, XRD, FE-SEM and thermal analysis (TGA-DTA). The pathogenic activities of the synthesized ligand (BIAB) was tested in vitro against the sensitive organisms *Staphylococcus aureus* (Gram-positive) and *Escherichia coli* (gram-negative) as antibacterial and *Aspergillus Niger* and *Candida albicans* as antifungal. The activity data show that the ligand (BIAB) higher antibacterial and slightly antifungus activity in comparison to the standard antibacterial (*Amoxicillin*) and antifungal (*cycloheximide*) drugs. The acute toxicity studies ($LD_{50}$) was calculated using by Miller and Tainter methods (Estimated Probity Units) for the calculation of $LD_{50}$. In this study, different doses (600, 1000, 1300, 1800, 2500 and 3600 μg/ml) of the (BIAB) was administered orally to the different groups of mice. The results exhibited high acute toxicity with $LD_{50}$ of 1020.23 mg/kg upon intraperitoneal administration in mice. The antioxidant properties of the ligand was examined using the DPPH radical scavenging technique. $IC_{50}$ was also determined at 224.17 μg/ml.

## 1. Introduction

During 1916–1920, G.N. Lewis and I. Langmuir, who proposed that electron transfer would form ionic species, laid the foundations of modern chemical bonding theory. Once the bonds have formed, however, (often called a coordinate bond), they are not distinctive from a 'non-normal covalent bond [1, 2, 3]. It was often proposed that one of such atoms has shared electrons in bonds. In biological systems (for example, heme and chlorophyll), certain essential forms of coordinated compounds occur [4]. The imidazole and derivatives characterized ligands azo dyes of heterocyclic compounds as highly effective against most of the elements of the periodic table as chemistry complexes. Using azo imidazolyl azo in different fields have been used in medicine, science and technology, giving results are of great importance in life [5, 6]. We are now in the process of developing heterocyclic azo mixtures. The central fragment of various natural and biological structures is has been formed by different imidazole derivatives that are an essential class of heterocycles [7]. Due to their strong biological activity, they hold a

* Corresponding author.
*E-mail address:* husseinkyhoiesh@gmail.com (H.A.K. Kyhoiesh).

https://doi.org/10.1016/j.heliyon.2021.e07969
Received 19 May 2021; Received in revised form 23 August 2021; Accepted 8 September 2021

special role in the field of medical chemistry [8]. One of the most studied organic compounds contains heterocyclic nitrogen, mostly because of its significance in the pharmaceutical [9] and chemical industries [10]. Although inorganic heterocyclic compounds can exist, they usually require one or more elements in the ring structure, such as sulfur, oxygen or nitrogen [11]. As the number of non-carbons substituted by carbon atoms is most generally assumed to be heteroatomic compounds [12]. The aromatic and non-aromatic rings can be used for the structures. The derivatives can be divided into two broad areas as a bunch of heterocyclic materials: aromatic and non-aromatic [13].

The chelation of Ag(I), Cu(II), Zn(II), Cd(II), Hg(II), and Pb(II) with CPLs based on Merrifield resin containing the imidazolylazobenzene (I) and 1,4-bis(imidazolylazo)benzene (II) chelating fragments is of particular interest. The development of five-membered chelate nodes requires the participation of azo-nitrogen and pyridine-nitrogen in the chelation process [14].

A wide range of chemical compounds, including those vital to human survival, such as vitamins and minerals, as well as medications, affect human health. Natural ingredients, by definition, have superior properties in terms of potency and stability when it comes to human wellbeing. Owing to the difficulty of meeting the global demand for natural materials due to their scarcity in nature, it is necessary to manufacture synthetic substances in significant amounts. This may include so-called nature equivalent compounds, which are natural molecules synthesized in an identical or slightly modified molecular structure to boost the molecule's biological function. Heterocycles are one of the most common scaffolds used in medicines and other pharmaceutically related substances. Heterocyclic nuclei's extraordinary capacity to function as biomimetic and reactive pharmacophores has primarily led to their special importance as conventional primary ingredients in a variety of medications. In modern drug research, the use of heterocycles as scaffolds with a high degree of diversity has become a major priority [13, 14, 15, 16].

In our present work, we report the measurements of 1,4-Bis(imidazolylazo)benzene, spectral characterisation and $LD_{50}$ (BIAB). Preparation of the substance (BIAB), studied with various spectral methods, (TGA-DTA), $^{1}$H-NMR, $^{13}$C-NMR, Mass, UV-Vis, Infrared FT-IR, XRD, FE-SEM, and C.H. N.

## 2. Materials and methods

### 2.1. Chemicals and solvents

The syntheses were carried out with analytical reagent grade chemicals and solvents, and they were utilized without additional purification. provided fine chemicals such as Imidazole, 1,4-diaminobenzene, Sodium nitrite, 1,1-Diphenyl-2-picrylhydrazyl (DPPH), HCl, NaOH, DMSO, DMF, EtOH, MeOH, Deionized water, Amoxicillin, cycloheximide, MS (mannitol salt) and potato dextrose (PDA) agars were purchased from commercial suppliers (B.H.D (England), Sigma-Aldrich (Germany), Honeywell Fluka (UK), Scharlu (España), and others.

### 2.2. Physical measurements

Elemental microanalyses of ligand (BIAB) was determined using EA 300 (C.H.N.S) Element analyzer. The $^{1}$H & $^{13}$C NMR spectra were obtained on a Bruker 400 MHZ spectrometer in DMSO-$d_6$ as the solvent, using TMS as the internal reference. Mass spectra of ligand (BIAB) was recorded using a Shimadzu Agilent Technologies 5973C at (70 eV). The electronic spectra were measured on a T80-PG double beam (UV-Vis) spectrophotometer in absolute ethanol using a quartz cuvette of 1 cm path length in the range of 200–1100 nm. FT-IR spectra (KBr disks, 4000–400 $cm^{-1}$) were recorded using a Shimadzu 8400 S. X-ray diffraction (XRD) measurements were performed using a Bestec Aluminium anode-Germany X-ray diffractometer with (Cu Kα) radiation (λ = 1.5418 °A) in the range of (20–80°)Θ. Thermal analysis (TGA-DTA) were investigated with a PL-TG instrument from 25 to 900 °C under a nitrogen atmosphere with a heating rate of (10 °C $min^{-1}$). Field emission scanning electron microscopy (FE-SEM) images were obtained on a MIRA3 TESCAN. The SMP, Stuart instrument was applied for the recording of the melting point or decomposition temperature of the ligand, capillary tube. The pH measurements were performed with a Philips PW 9421. The compound was created using PerkinElmer ChemBioDraw software and then optimized using PerkinElmer ChemBio3D software.

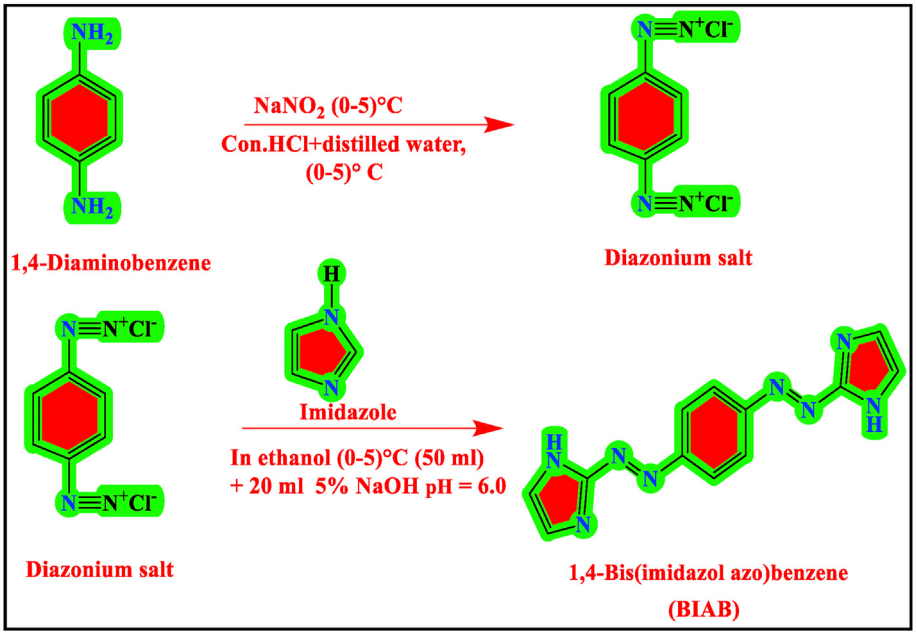


**Figure 1.** Synthesis of azo ligand 1,4-Bis(imidazolylazo)benzene (BIAB).

### 2.3. Synthesis of 1,4-Bis(imidazolylazo)benzene (BIAB)

The ligand (BIAB) was synthesized by the following methods suggested by Al-Adilee et al. [17, 18] has included the new heterocyclic 1,4-Bis(imidazolylazo)benzene (BIAB) with some revision Figure 1. Dissolving 1.8 g (0.01 mol) of 1,4-diaminobenzene in 25 mL distilled water and 4 mL of concentrated hydrochloric acid (HCl) was used to produce a diazonium solution. A beaker was placed in an ice bath, and the contents of the beaker stirred, cooling up (0–5) °C to the filtered solution. In a combination of 25 ml distilled water a solution of 1.4 g (0.02 mol) of sodium nitrite ($NaNO_2$) (0–5) °C was added to the mixture and aged for around 30 min. With cooling and constantly ripening at (0–2)°C the resulting diazonium chloride solution was applied to a 500 mL beaker containing 1.6 g (0.02 mol) of imidazole dissolve in 50 mL of ethanol and 20 ml of 7% sodium hydroxide was ripened for 3 h in an ice-bath and acidification with dilutes of hydrochloric acid pH = 6,0 at (0–5)°C in ice-bath. The raw product was filtered out, distilled water cleaned, purified from ethanol and dried by recrystallization. The obtained 1,4-bis(imidazolylazo)benzene (BIAB) was eventually dried for several hours in the oven at 50 °C and is held in a desiccator by anhydrous dryers. The reaction yield was 70%, and its color was purple crystals and m.p = 229 °C. $^1$H-NMR (400 MHz, DMSO-*d*6) δ 12.24 (s, 2H, N–H), 7.64 (s, 4H, C-$H_{\text{benzene ring}}$), 7.11–6.89 (m, 4H, C-$H_{\text{imidazole ring}}$), 2.52 (s, solvent DMSO). FT-IR, υ(N–H) 3202cm$^{-1}$, υ(C-$H_{\text{aromatic}}$) 3090 cm$^{-1}$, υ(C–H $_{\text{aliphatic}}$) 2861 cm$^{-1}$, υ(C=N) 1628 cm$^{-1}$, υ(N=N) 1437 cm$^{-1}$, υ(C=N) 1628 cm$^{-1}$, υ(C–N)$_{\text{Imidazole}}$ 1250 cm$^{-1}$ and 794 cm$^{-1}$, υ(C–N=N–C) and υ(C=N–N=C) 1339 cm$^{-1}$, 1317 cm$^{-1}$ and 679 cm$^{-1}$ *m/z*: calculated for $C_{12}H_{10}N8$ (266.268). C.H.N.S, X-ray, TGA-DTA, FE-SEM and UV-Visible spectra explained the molecular composition of 1,4-Bis (imidazolylazo) benzene. The following Figure 1 summarizes the 1,4-Bis(imidazolylazo)benzene method of preparation (BIAB).

### 2.4. Microbiological investigation

In this study, two different species of gram-positive and negative bacteria with the sensitivity test system were examined on the inhibitory biological effects of the compounds prepared. The test bacteria is *Staphylococcus aureus* (MTCC 3160) and *Escherichia coli* (MTCC 723). Furthermore, the antifungal activates were tested against (*Aspergillus niger*) (MTCC 1881) and (*Candida albicans*) (MTCC 3958). Nutrient Broth, Mueller Hinton and potato dextrose (PDA) agars were used. The technique (Gram's Method) was also used to diagnose bacteria [19, 20]. Inhibitory zone diameters were measured after 24 h and 7 days, for bacteria and fungi, respectively. The antibacterial and antifungal activities were done at 100 μg/mL concentrations in DMSO solvent by the agar diffusion method. The usual antibacterial and antifungal drugs were *amoxicillin* and *Cycloheximide*, respectively.

### 2.5. Animals

Lab mice (25–30 g) were utilized after being acclimatized in laboratory conditions for 7 days and were typical of similar age (10–12 weeks). The animals had access to food and water, and the sun and dark cycles were shorter than the 12:12 LD cycle. Temperatures of 65–75°F (18–23 °C) with 40–60% humidity.

### 2.6. Acute toxicity studies

The acute toxicity investigations were carried out using the usual approach by Miller and Tainter [21, 22, 23] using the method (Estimation of probity units), in which male albino mice were divided into six groups, each containing ten animals ($LD_{50}$ determination). The ligand dosages were reduced by half in each group $\sqrt{1/2}$ (3600, 2500, 1800, 1300, 1000, and 600 mg/kg body weight). The lethal dose for half of the animals was determined by administering these concentrations orally via an infected tube and recording the indications of poisoning and death within 24 h (LD50).

The animals were kept under constant observation for the first 2 h and then every 4 h after that. There were reports of death and surviving animals after 24 h. The LD50 was calculated both technically and graphically. First, the death percentage was computed using the calculation below, and then the ratio was modified to 0 % and 100 % (Eqs. (1) and (2)) [24, 25];

$$\text{For 0\% death} = 100 \times (0.25/n) \quad (1)$$

$$\text{For 100\% death} = 100 \times [(n - 0.25)/n] \quad (2)$$

where n is the number of animals in each category.

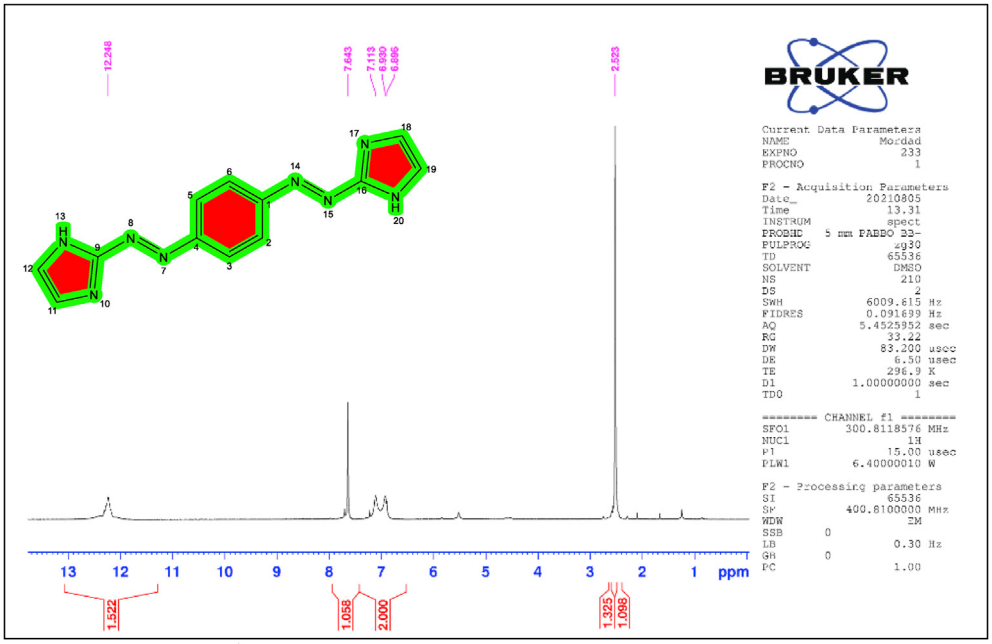


**Figure 2.** $^1$H-NMR spectrum of 1,4-Bis(imidazolylazo)benzene (BIAB).

**Table 1.** Assignment of the $^{13}$C-NMR spectrum of the ligand (BIAB).

| BIAB | | |
|---|---|---|
| Chemical Shift (ppm) | Position | Associated group |
| 130.56 | $C_9$ | -imidazole-C |
| 130.35 | $C_{16}$ | -imidazole-C |
| 124.17 | $C_1$ | -Ar-C |
| 123.96 | $C_4$ | -Ar-C |
| 123.40 | $C_{11}$ | -imidazole-C |
| 123.00 | $C_{12}$ | -imidazole-C |
| 119.68 | $C_{18}$ | -imidazole-C |
| 118.80 | $C_{19}$ | -imidazole-C |
| 116.48 | $C_7$ | -Ar-C |
| 116.38 | $C_9$ | -Ar-C |
| 116.11 | $C_{17}$ | -Ar-C |
| 116.00 | $C_{18}$ | -Ar-C |
| 39.11–40.78 | - | DMSO-d6 |

### 2.7. DPPH radical scavenging assay

The ligand's antioxidant activity (BIAB) is measured by its ability to scavenge the stable free radical 2,2-diphenyl-1-picrylhydrazyl (DPPH). As the color changes from purple to yellow, the stable free radical DPPH displays an electrical absorption band limit at 517 nm. When the odd electron of the DPPH radical is combined with hydrogen from a free radical scavenging antioxidant to form reduced DPPH, the absorption band narrows [26]. A 0.3mM DPPH solution was produced in DMSO and applied to the ligand in 1 mL at different concentrations (0, 25, 50, 100, 200, and 400 μg/mL). The reaction mixture was continuously stirred and kept at 25 °C in the dark for 60 min. At 517nm, the absorbance of the produced reaction mixture was measured, with ascorbic acid as a positive control. This was done with three replications for each concentration. The percentage of DPPH radicals scavenged was determined using the formula below (equation 3) [27];

$$SCV\% = \left(\frac{A_{control} - A_{sample}}{A_{Control}}\right) \times 100 \quad (3)$$

where $A_{Control}$ is the absorbance of the control reaction (containing all reagents except the test compound) and $A_{Sample}$ is the absorbance of the test compound. The $IC_{50}$ value, known as the concentration of sample required to induce 50% inhibition, was calculated by plotting the percentage of DPPH-scavenging activity against the sample concentration.

## 3. Result and discussion

### 3.1. Characterization of 1,4-Bis(imidazolylazo)benzene (BIAB)

The BIAB, 1,4-Bis(imidazolylazo)benzene, was purple crystals. In certain organic solvents, including ammonia, methanol, ethanol, acetone, DMF and DMSO, ligand (BIAB) is stable and soluble and is soluble in water. The experimental result of the simple study of prepared 1,4-Bis(imidazolylazo) benzene (BIAB) is consistent with the theory. In order to test the purity of the azo dye (BIAB), elemental analysis C.H.N.S is used. Elemental analyses of the bis(imidazolylazo)benzene show that the carbon present within the (BIAB) is 54.06% and hydrogen contain (3.92%). Similarly, the nitrogen content in the (BIAB) is 42.02 %, which is entirely owing to the integrated nitrogenous functional group, according to the elemental analysis of ligand azo.

### 3.2. $^{1}$H-NMR spectra

The ligand 1,4-Bis(imidazolylazo)benzene (BIAB) proton magnetic resonance spectrum ($^{1}$H-NMR) was calculated as a TMS as an internal reference (400 $_{MHZ}$) with DMSO-$d^6$ as a solvent and the following peaks were observed in Figure 2. The free ligand spectrum (BIAB) showed the low field signal at δ = 12.24 ppm (s,2H) due to the existence in positions 13 and 20 of the imidazole group (N–H). At the same time, the (BIAB) ligand showed a signal at δ = 7.64 ppm (s,4H of benzene ring) at positions 2,3,5 and 6. A signal at δ = 6.89–7.11 ppm (m, 4H of imidazole ring

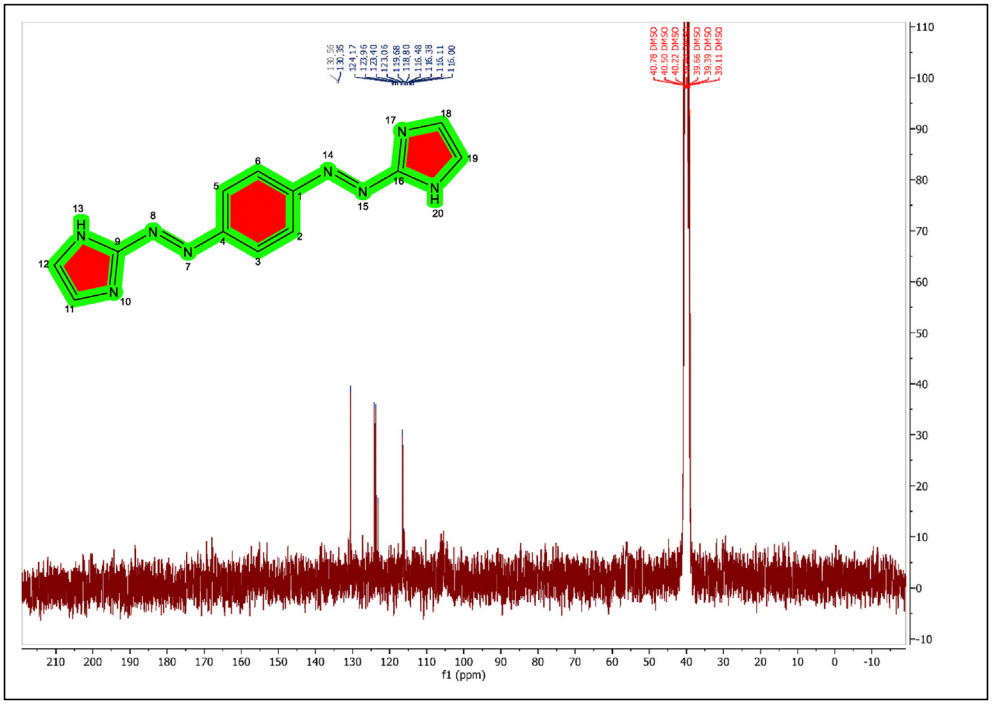


**Figure 3.** $^{13}$C-NMR spectrum of the ligand (BIAB).

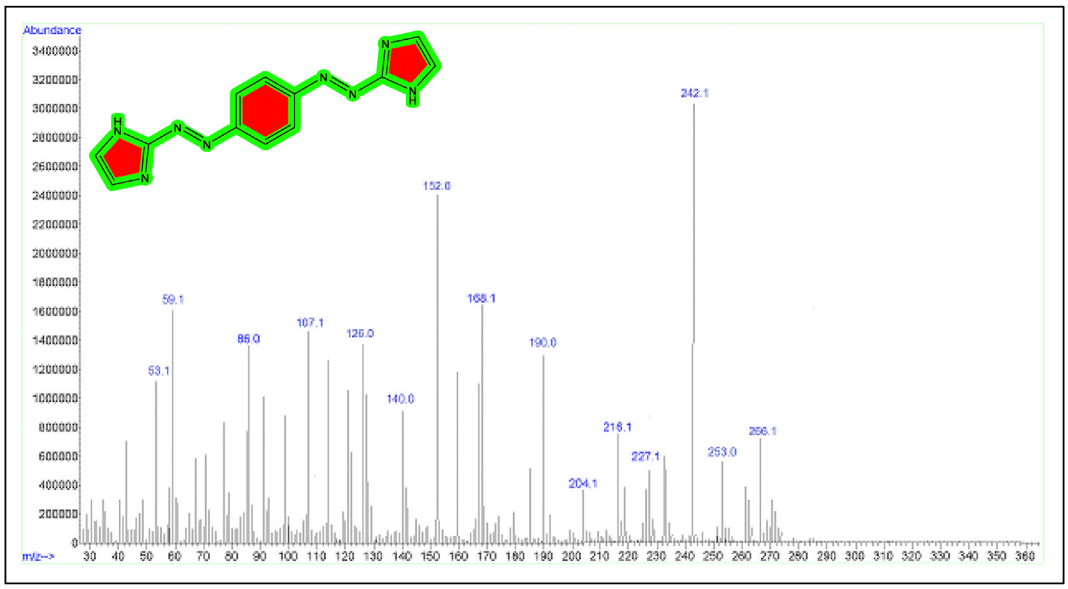


**Figure 4.** Mass spectrum of ligand (BIAB).

**Table 2.** Physical properties and elemental analysis for ligand (BIAB).

| Compound | Color | m.p C° | Optimal pH | Yield % | Molecular Formula (M.wt) (g/mol) | Found% (Calc.) | | | |
|---|---|---|---|---|---|---|---|---|---|
| | | | | | | C% | H% | %N | %M |
| BIAB | purple | 229 | 6.5 | 70 | $C_{12}H_{10}N_8$ (266.268) | 54.06 (54.13) | 3.92 (3.79) | 42.02 (42.08) | – |

**Table 3.** The spectral data of the azo dye ligand (BIAB).

| Compound | $\lambda_{max}$ (nm) | Absorption bands($cm^{-1}$) | Transitions |
|---|---|---|---|
| BIAB | 374 | 26738 | n →π* |
| | 291 | 34364 | π →π* |

proton) at positions 11, 12, 18 and 19. Although the signal at δ = 2.52 ppm (s, solvent proton) is due to the influence of DMSO solvent [28].

### 3.3. $^{13}$C-NMR spectra

The $^{13}$C-NMR of the (BIAB) was investigated, and signals were observed due to the presence of various carbon atom types. Table 1 and Figure 3 show the assignment of the $^{13}$C-NMR spectra of the (BIAB).

### 3.4. Mass spectral analysis

The mass spectrum can be utilized to confirm the ligand's structure as well as its complexes. Multiple peaks were seen in the fragmentation ligand (BIAB) mass spectrum (Figure 4). Table 2 lists all of the mass spectrum data in detail. The mass spectrum of the novel ligand (BIAB) display a base peak at m/z+ = $C_{12}H_{10}N8$ (266.1), which is ascribed to the ligand's original molecular weight (BIAB) (266.268), [$C_{12}H_{10}N8$] (19.87%). This data matches the chemical formulas well. Figure 4 illustrate the pattern of ligand (BIAB).

### 3.5. Electronic spectral studies

In the fresh ethanol solution ($10^{-3}$M) at room temperatures, the electronic absorption spectrum of 1,4-bis(imidazolylazo)benzene (BIAB) was reported. Table 3 summarizes the spectral details from the azo dye ligand (BIAB). The free ligand electronic spectrum is distinguished by two U.V-visible absorptions. These bands are 291 nm (34364 cm-1) and

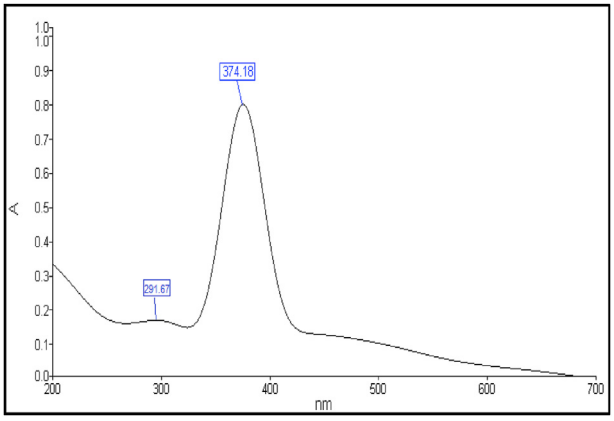


**Figure 5.** UV-visible spectra of ligand (BIAB).

374 nm (26738 $cm^{-1}$). A transition from π →π* within the imidazole ring is the primary band. Although n →π* transition was due for the second band, the existence of a band with a double bond resulted, Besides hetero atom, an ion-pair electron, such as (=C=N-), in addition to the intermolecular charge transfer in the imidazole ring were also present from the phenyl ring into the azo group (-N=N-) into the imidazole ring [29, 30]. Azo dye ligand (BIAB) UV-visible spectra are seen in Figure 5 and Table 3.

### 3.6. Infrared spectra

Spectral infrared data (KBr disk) of 1,4 Bis(imidazolylazo)benzene (BIAB) (Table 4). The υ(N–H) imidazole ring has been assigned to a broad 3202$cm^{-1}$ in the FT-IR range of the free bisazo ligand [31, 32]. The band stays in the same free ligand region (BIAB). The ligand (BIAB) spectrum is typical of two strong bands with an aromatic and aliphatic value of 3090

**Table 4.** Characteristic FT-IR absorption bands of the ligand (BIAB) in $cm^{-1}$ units (KBr disc).

| Group | Ligand |
|---|---|
| υ (N–H) | 3202 Vs. |
| υ $(C–H)_{Aromatic}$ | 3090 s. |
| υ $(C–H)_{aliphatic}$ | 2861 s. |
| υ (C=N) and υ $(C–N)_{Imidazole}$ | 1628 s. 1250 w. 794 w. |
| υ (N=N) | 1437 s. |
| υ(C=C) | 1383 m.<br>756 w. |
| υ(C–N=N–C) and υ(C=N–N=C) | 1339 m.<br>1317 m. 679 w. |

Vs = very strong, s = strong, m = medium, w = weak, sh = sholder, br = broad.

$cm^{-1}$ and 2861 $cm^{-1}$, respectively. The medium band found in the free ligand at 1628 $cm^{-1}$ was credited to υ (C=N) stretch of the azomethine (C=N). The azo group υ (N=N) stretch was attributed to a medium-intensity band at 1437 $cm^{-1}$. The υ (C=N) and υ $(C–N)_{Imidazole}$ stretching vibration appears at 1628 $cm^{-1}$, 1250 $cm^{-1}$ and 794 $cm^{-1}$ respectively. The IR spectra of ligand (BIAB) appear bands at 1339 $cm^{-1}$, 1317 $cm^{-1}$ and 679 $cm^{-1}$ due to υ(C–N=N–C) and υ(C=N–N=C) the presence of diazo group with the conjugated system. The azo dye ligand (BIAB) infra-red spectrum is seen (Figure 6).

### 3.7. X-ray diffraction study (XRD)

The intensity of diffracted CuKα radiation was calculated in 2Θ between 0° and 80° (k = 0.1542 nm; 50 kV and 40 mA). The (XRD) 1,4-Bis (imidazolylazo)benzene (BIAB) patterns appear in this section (Figure 7). A very high degree of crystallinity was shown in the XRD analysis of the prepared (BIAB). Because of the range of high-population x-ray diffraction (BIAB), because of micro-strain and cracking crystalline collapse, as a result of crystalline-scale distortion and domain crystals and domain size distribution [33], it reflects an indicated crystalline nature structure. Bragg's Eq. (4) was used to measure the spacing of reflections [17, 34];

$$n\lambda = 2d\sin\theta \quad (4)$$

where (d) is the spacing between the crystalline levels, (n) is an integer (1,2,3 ...), (λ) is the wavelength of X-ray CuKα = 1.540598 A°, (Θ) is the diffraction angle. The d-spacing values and the following data show each peak's 2Θ values and its relative intensity (Table 5). The findings revealed that the d-spacing of 2.81485 A° suggested the crystalline state of 1,4-Bis (imidazolylazo)benzene (BIAB) with 14 reflections with a maximum of 2Θ = 31.764°. Crystal sizes (BIAB) have been calculated in the Debye– Scherrer Eq. (5) [30, 35];

$$D = k\lambda/\beta\cos\theta \quad (5)$$

where (D) is the volume average diameter of the crystallite, (k) is Blank's constant (0.891), (λ) is the X-ray wavelength (0.15405 nm), and (Θ) and (β) are the diffraction angle and full width at half maximum of a reported peak, respectively. It was determined the average crystallite size (D) for (BIAB). The following relationship Eq. (6) [36] was well determined for the dislocation density (δ);

$$\delta = 1/D^2 \quad (6)$$

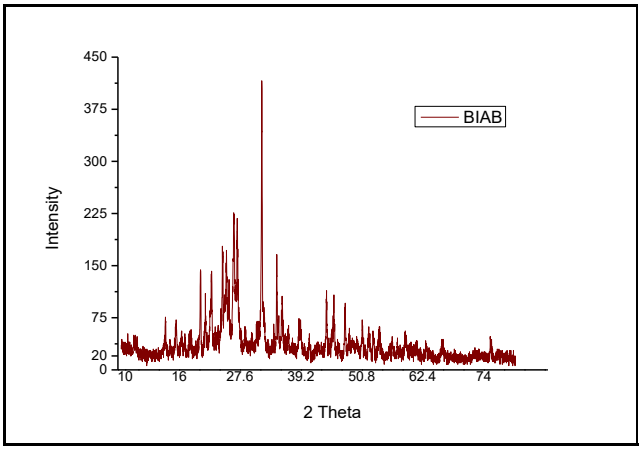


**Figure 7.** XRD patterns of 1,4-Bis(imidazolylazo)benzene (BIAB).

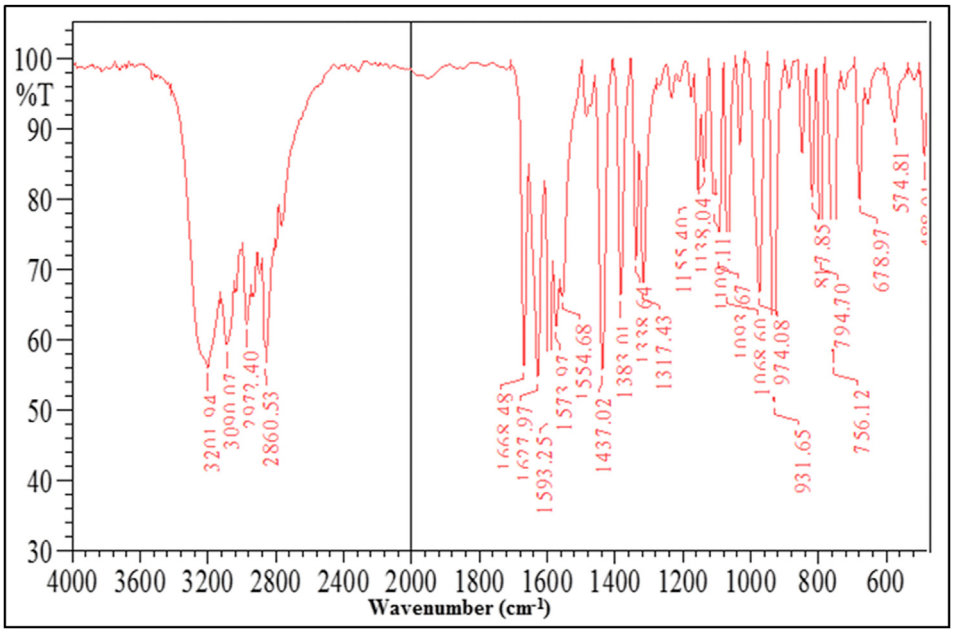


**Figure 6.** FT-IR Spectrum of ligand (BIAB).

**Table 5.** Crystallographic data for (BIAB).

| Compound | Peak no. | °2Θ(degree) | d Spacing (A°) | Intensity (I/I◦)% | FWHM [°2Θ] | Crystallite Size D (nm) | Lattice Strain | Dislocation density δ X $10^{-4}$ $(nm)^2$ |
|---|---|---|---|---|---|---|---|---|
| BIAB | 1 | 20.129 | 4.40786 | 32 | 0.17700 | 47.63 | 0.0044 | 4.407 |
| | 2 | 22.203 | 4.00050 | 28 | 0.23700 | 35.69 | 0.0053 | 7.850 |
| | 3 | 24.314 | 3.65771 | 32 | 0.20050 | 42.35 | 0.0041 | 5.575 |
| | 4 | 25.043 | 3.55284 | 29 | 0.22570 | 37.68 | 0.0044 | 7.042 |
| | 5 | 25.534 | 3.48573 | 18 | 0.14120 | 60.27 | 0.0027 | 2.757 |
| | 6 | 26.448 | 3.36732 | 45 | 0.33030 | 25.82 | 0.0061 | 1.499 |
| | 7 | 27.121 | 3.28516 | 41 | 0.22450 | 38.04 | 0.0041 | 6.910 |
| | 8 | 31.764 | 2.81485 | 100 | 0.17600 | 49.04 | 0.0027 | 4.158 |
| | 9 | 34.613 | 2.58933 | 35 | 0.14620 | 59.47 | 0.0020 | 2.827 |
| | 10 | 35.657 | 2.51591 | 18 | 0.13780 | 63.28 | 0.0019 | 2.497 |
| | 11 | 41.501 | 2.05345 | 25 | 0.15770 | 52.64 | 0.0018 | 3.608 |
| | 12 | 45.475 | 1.99295 | 24 | 0.14480 | 62.16 | 0.0015 | 2.588 |
| | 13 | 47.581 | 1.90955 | 18 | 0.19150 | 47.37 | 0.0019 | 4.456 |
| | 14 | 75.279 | 1.26135 | 10 | 0.17340 | 60.44 | 0.0010 | 2.737 |

**Table 6.** Crystallographic parameters for (BIAB).

| Characteristic | Data and Conditions |
|---|---|
| Formula | $C_{12}H_{10}N_8$ |
| Crystal colour | Purple |
| M.wt | 266.268 |
| Crystal system | Cubic |
| Space group | Fm3m |
| Space group number | 225 |
| a (A°) | 5.6402 |
| b (A°) | 5.6402 |
| c (A°) | 5.6402 |
| Alpha (°) | 90.0000 |
| Beta (°) | 90.0000 |
| Gamma (°) | 90.0000 |
| Calculated density (g/cm3) | 2.16 |
| Measured density (g/cm3) | 2.17 |
| Volume of cell (10⁶ pm3) | 179.43 |
| Z | 4.00 |
| RIR | 4.40 |
| Reference code | 00-005-0628 |

where (δ) is dislocation density, (D) is the average grain size. In Figure 6, the histogram of the particle size distribution (BIAB) has been shown and (Tables 5 and 6).

### 3.8. Thermal analyses

Thermogravimetric analysis (TGA) and differential thermal analysis (DTA) was identified with ligand curves (BIAB) (Figure 8). The results of ligand thermogravimetric (BIAB) analyzes are recorded (Table 7). The thermograms were performed in an oxygen atmosphere at 10 °*C min*$^{-1}$ within the range of 22–800 °C. The TGA curve shows three phases of decomposition of the ligand (BIAB) of the formula ($C_{12}H_{10}N_8$). The first step inside the temperature range of 22–243 °C is the moisture and volatile materials, which reflected mass losses of 6.62%. The second decomposition step within the 243–418 °C range corresponds to the loss ($C_8H_5N_7$) of 74.85 % in these processes. The final decomposition step within the 418–1000 °C range is the loss of further complete fragmentation of a ligand (BIAB), with mass losses of 10.60% at the same time. The peaks of the DTA curve were 200, 335 °C leaving as residue carbon [37, 38].

### 3.9. FE-SEM analysis

The Field emission scanning electron microscopy (FE-SEM) ligand (BIAB) investigates surface morphology, particulates form, aggregation and propagation of these particles. At 1μm cross-sectional length and a magnification force of Mag = 30.00 KX, a scanning microscope technology was used. The FE-SEM picture was demonstrated in (Figure 9). The ligand (BIAB) shaped peripherally of the spherical shapes at an average size 92 nm with a ratio of less than totality is seen in the FE-SEM image. FE-SEM demonstrated that in some cases, the particles became agglomerated and non-uniform [39]. Nanoparticles with different sizes and morphology have been synthesized in various conditions e.g. isolated particle (100–150 nm), aggregate particles (600–700 nm), irregular multilateral shapes (1.5–2 μm), porous structure (40 nm), and nanoparticles (28–32 nm) [40]. Controlling shape, particle size, and size distribution, as well as developing novel functionalization processes, are all important elements in effectively implementing nanoparticles in various applications [41]. Thermal decomposition techniques, for example, provide an alternative to the regularly used co-precipitation approach for producing nanoparticles with a regulated form, adjustable size, and limited size distribution, giving them distinctive features [42]. The pyrolysis preparation technique and reaction conditions must be modified or revised in order to create consistent nanosized materials. For example, atomizing the precursor solution with ultrasonic waves [43], dispersing the precursor solution with a stable matrix such as zeolite [44] or glass, slowing the reaction rate to obtain nanoparticle films, i.e., the oxide superconducting films formed in vacuum, authorizing the reaction to occur in an inert solvent or inert gas, and using up decomposable polymers or molecules [45]. These changes effectively lower the nanoparticles' crucial formation temperature. They also prevent aggregation and agglomeration of the nanoparticles [46, 47].

### 3.10. Antimicrobial activity

The ligand (BIAB) was examined in vitro against bacteria gram-positive (*Staphylococcus aureus)*, gram-negative *(Escherichia coli),* antifungal *(Aspergillus niger*) and (*Candida albicans)* at the concentration 100 μg/ml shown in Table 8 and Figure 10. Ligand (BIAB) showed direct antibacterial and antifungal activities in comparison to the standard antibacterial (*Amoxicillin*) and antifungal (*cycloheximide*) drugs. Data revealed that 1,4-bis (imidazolylazo)benzene (BIAB) is more effective relative to other bacteria and fungi in *Escherichia coli* strains. The *Escherichia coli* bacteria displayed a high susceptibility to the ligand. The findings showed that the form of compensated compound groups, for

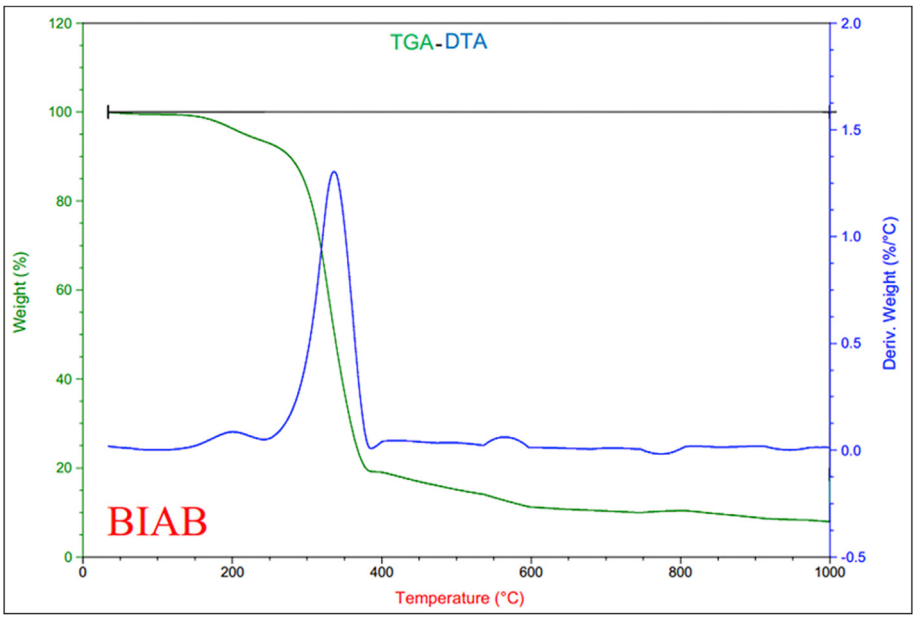


**Figure 8.** TGA-DTA curves of ligand (BIAB).

**Table 7.** Thermoanalytical data (TGA-DTA) of ligand (BIAB).

| Compound | TG Range (°C) | Mass loss% Found(Calc.) | Assignment | DTA (°C) | Residue |
|---|---|---|---|---|---|
| (BIAB) | 22–243 | 6.62 (6.40) | Evolution of moisture and ($C_1H_5$) | 200 | _ |
| | 243–418 | 74.85 (74.80) | Loss ($C_8H_5N_7$) | 336 | |
| | 418–1000 | 10.60 (10.59) | Loss of a part of the ligand | | |

example, the group (-N=N- and N–H), in the studied ligand [48, 49, 50], influence the degree of efficacy and the bacteria type influencing them. Fungi, on the other hand, indicated that the majority of the compound tested had moderate to weak active ingredients (inhibition zones ranged from 6 to 9 mm) [51].

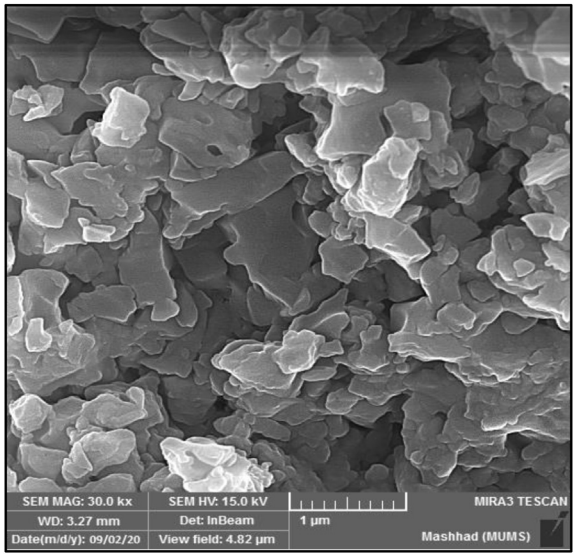


**Figure 9.** FE-SEM images of ligand (BIAB).

**Table 8.** Antimicrobial activity data (zone of inhibition in mm) of azo dye ligand (BIAB).

| Compound | Bacteria | | Fungi | |
|---|---|---|---|---|
| | Gram Positive | Gram Negative | | |
| BIAB | *Staphylococcus aureus* | *Escherichia coli* | Aspergillus Niger | *Candida albicans* |
| | 13 mm +++ | 18 mm +++ | 6 mm + | 9 mm ++ |
| *Amoxicillin* | 19 +++ | 15 +++ | — | — |
| *Cycloheximide* | — | — | 16 +++ | 10 ++ |

Highly active = + + + (inhibition zone >12 mm).
Moderately active = + + (inhibition zone 9–12 mm).
Slightly active = + (inhibition zone 6–9 mm).
Inactive = - (inhibition zone <6 mm).

### 3.11. Acute toxicity of (BIAB)

The results for acute toxicity studies ($LD_{50}$ determination) are tabulated as shown in Tables 9, 10, 11 and Figures 11, 12. The toxicity determinations were carried out in which % mortality observed was 0, 0, 20, 50, 80 and 100%, respectively, for the doses corresponding to 600,

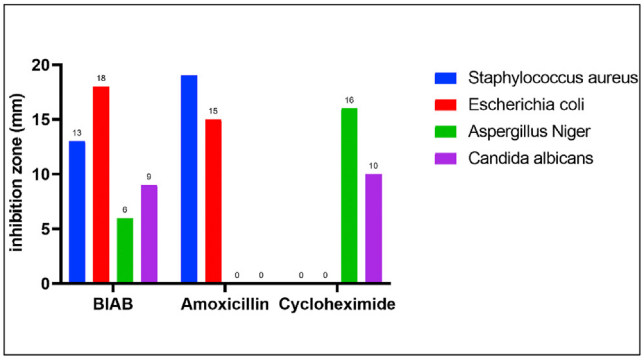


**Figure 10.** Antimicrobial Activity of ligand (BIAB).

**Table 9.** Miller & Tainter method of estimation of LD50 [43].

| % | 0 | 1 | 2 | 3 | 4 | 5 | 6 | 7 | 8 | 9 |
|---|---|---|---|---|---|---|---|---|---|---|
| 0 | - | 2.67 | 2.95 | 3.12 | 3.25 | 3.36 | 3.45 | 3.52 | 3.59 | 3.66 |
| 10 | 3.72 | 3.77 | 3.82 | 3.87 | 3.92 | 3.96 | 4.01 | 4.05 | 4.08 | 4.12 |
| 20 | 4.16 | 4.19 | 4.23 | 4.26 | 4.29 | 4.33 | 4.36 | 4.39 | 4.42 | 4.45 |
| 30 | 4.48 | 4.50 | 4.53 | 4.56 | 4.59 | 4.61 | 4.64 | 4.67 | 4.69 | 4.72 |
| 40 | 4.75 | 4.77 | 4.80 | 4.82 | 4.85 | 4.87 | 4.90 | 4.92 | 4.95 | 4.97 |
| 50 | 5.00 | 5.03 | 5.05 | 5.08 | 5.10 | 5.13 | 5.15 | 5.18 | 5.20 | 5.23 |
| 60 | 5.25 | 5.28 | 5.31 | 5.33 | 5.36 | 5.39 | 5.41 | 5.44 | 5.47 | 5.50 |
| 70 | 5.52 | 5.55 | 5.58 | 5.61 | 5.64 | 5.67 | 5.71 | 5.74 | 5.77 | 5.81 |
| 80 | 5.84 | 5.88 | 5.92 | 5.95 | 5.99 | 6.04 | 6.08 | 6.13 | 6.18 | 6.23 |
| 90 | 6.28 | 6.34 | 6.41 | 6.48 | 6.55 | 6.64 | 6.75 | 6.88 | 7.05 | 7.33 |

**Table 10.** Transformation table for the dose to probits.

| (Probits) | (Corrected %) | (% dead) | (Md) | Log dose | (dose) (mg/kg) | (n) | Group |
|---|---|---|---|---|---|---|---|
| 3.04 | 2.5 | 0 | 0 | 2.477 | 600 | 10 | 1 |
| 3.04 | 2.5 | 0 | 0 | 2.698 | 1000 | 10 | 2 |
| 4.16 | 20 | 20 | 2 | 2.845 | 1300 | 10 | 3 |
| 5.00 | 50 | 50 | 5 | 3.000 | 1800 | 10 | 4 |
| 5.84 | 80 | 80 | 8 | 3.113 | 2500 | 10 | 5 |
| 6.96 | 97.5 | 100 | 10 | 3.278 | 3600 | 10 | 6 |

Log Dose = 3.00087.
$LD_{50}$ = 1020.23 mg/kg.

**Table 11.** Fitted Line: l dose versus probit unit.

| Regression Analysis: l dose versus probit unit | | | | | |
|---|---|---|---|---|---|
| The regression equation is | | | | | |
| l dose = 2.068 + 0.1785 probit unit | | | | | |
| S = 0.0855727 R-Sq = 93.0% R-Sq(adj) = 91.3% | | | | | |
| Analysis of Variance | | | | | |
| Source | DF | SS | MS | F | P |
| Regression | 1 | 0.391700 | 0.391700 | 53.49 | 0.002 |
| Error | 4 | 0.029291 | 0.007323 | | |
| Total | 5 | 0.420991 | | | |

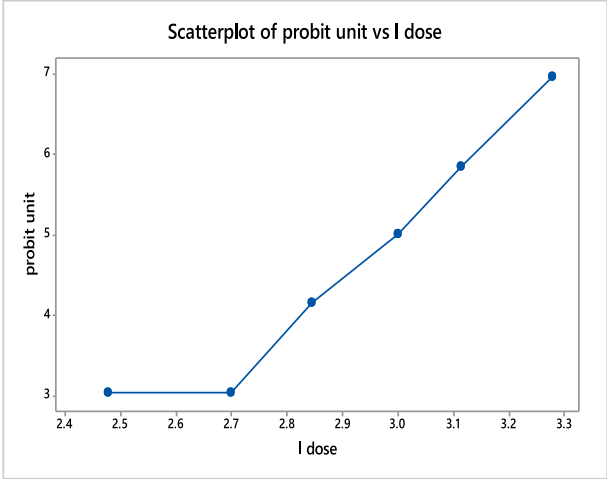


**Figure 11.** The dose-response graph in terms of probability units.

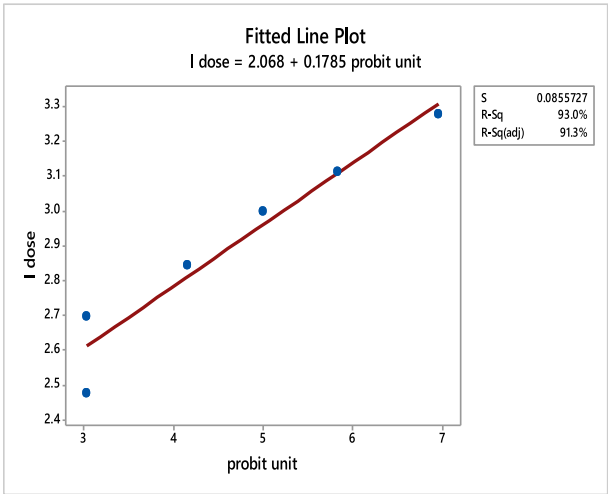


**Figure 12.** The straight line equation to describe the response.

**Table 12.** Results of antioxidant activity evaluation for BIAB and Ascorbic acid.

| Compound No. | Concentration (μg/ml) | | | | | $IC_{50}$ (μg/ml) |
|---|---|---|---|---|---|---|
| | 25 | 50 | 100 | 200 | 400 | |
| | % Antioxidant activity | | | | | |
| Ascorbic Acid | 39.65 | 50.79 | 85.32 | 99.21 | 99.77 | 42.43 |
| BIAB | 4.76 | 19.34 | 38.21 | 45.37 | 71.11 | 224.17 |

1000, 1300, 1800, 2500 and 3600 mg/kg, respectively. When a plot of log dose (on X-axis) vs. % mortality (on Y-axis) was plotted, a line was obtained, which at probit 5 extrapolated to a value of 3.00087 on X-axis, which in turn corresponds to the value of 1020.23. Thus the $LD_{50}$ of ligand BIAB was found to be 1020.23 mg/kg of the body weight. The drug is practically non-toxic at oral doses, supporting the fact that it was widely used in ancient ages [52, 53, 54, 55, 56]. Toxicity was observed with BIAB the death of all (100%) animals at 3600 mg/kg b.wt.

### *3.12. DPPH radical scavenging assay*

The DPPH assay is commonly used to determine the ability of a substance to scavenge free radicals and is calculated in terms of $IC_{50}$ values. In the visible field, DPPH has a high absorbance at 517 nm, which will be reduced when the ligand is added (BIAB). The azo group in the tested BIAB can be donated to the DPPH free radical [57]. When an odd electron on the DPPH radical is paired off in the presence of BIAB, it is reduced, and the colour of the solution varies from purple to yellow. The decrease in the absorbance value of DPPH at 517 nm can be used to

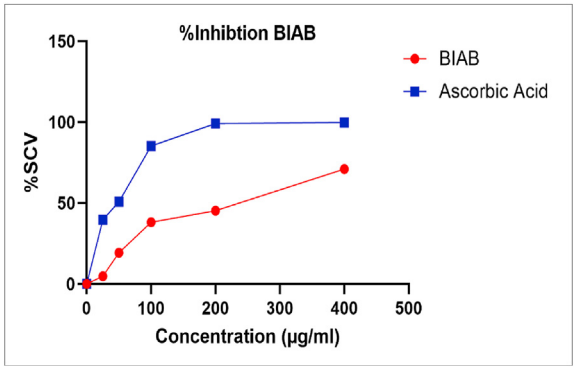


**Figure 13.** Antioxidant activity of BIAB.

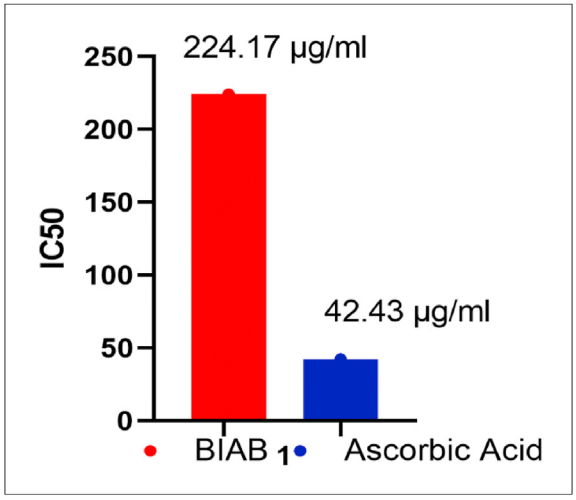


**Figure 14.** $IC_{50}$ for BIAB and Ascorbic acid.

calculate the BIAB's free radical scavenging function [58]. With increasing BIAB concentrations, scavenging activity increases. At 400 µg/ml, BIAB has a higher antioxidant activity. The findings (Table 12) and (Figures 13,14) show that BIAB outperforms standard ascorbic acid.

## 4. Conclusions

Azo dye ligand 1,4-Bis(imidazolylazo)benzene (BIAB) derived from imidazole was prepared and structurally characterized. The ligand structure and interpretation results (C.H.N), FT-IR, $^{1}$H-NMR and electronic spectra confirmed this formation. Azo dye ligand has many morphologies, as seen in XRD and FE-SEM, TGA-DTA of ligand (BIAB), as well as a good thermal stabilization result. The biological activity and the extraordinary biological activity of the synthesized BIAB ligand. The analysis indicates that the ligand is highly biological in effectively checked against *Escherichia coli, Staphylococcus aureus, Aspergillus Niger* and the *Candida albicans*. The activity data indicate that the highly active ligand is prepared against all testing species of bacteria. The lethal dose for half of the animal number ($LD_{50}$) of the organic compound (BIAB) was 1020.23 mg/kg, of the animal's weight. As for the half-maximal inhibitory concentration ($IC_{50}$) attain 224.17 µg/ml by examining free radicals.

## Declarations

### *Author contribution statement*

All authors listed have significantly contributed to the development and the writing of this article.

### *Funding statement*

This research did not receive any specific grant from funding agencies in the public, commercial, or not-for-profit sectors.

### *Data availability statement*

Data included in article/supplementary material/referenced in article.

### *Declaration of interests statement*

The authors declare no conflict of interest.

### *Additional information*

No additional information is available for this paper.

## Acknowledgements

Acknowledgments and thanks to Dr. Khalid Al-Adilee, for his encouragement and moral support during the scientific research.

## References

[1] L. Pauling, GN Lewis and the Chemical Bond, ACS Publications, 1984.
[2] R.E. Kohler Jr., The Lewis-Langmuir theory of valence and the chemical community, 1920-1928, Hist. Stud. Phys. Sci. 6 (1975) 431–468.
[3] J. Linnett, A modification of the Lewis-Langmuir octet rule, J. Am. Chem. Soc. 83 (12) (1961) 2643–2653.
[4] D. Garvin, G. Kistiakowsky, The kinetics of coordinate bond formation, J. Chem. Phys. 20 (1) (1952) 105–113.
[5] S. Granick, Evolution of Heme and Chlorophyll. Evolving Genes and Proteins, Elsevier, 1965, pp. 67–88.
[6] E. Catherine, Housecroft, sharpe AG, 4th ed, Inorg. Chem. (2012) 31–5.
[7] T. Mathur, J. Dinda, P. Datta, G. Mostafa, T.-H. Lu, C. Sinha, Ru (0)-azoimine-carbonyl and Ru (II)-pyridyl-azo-imidazole complexes, Polyhedron 25 (13) (2006) 2503–2512.
[8] S. Slassi, A. Fix-Tailler, G. Larcher, A. Amine, A. El-Ghayoury, Imidazole and azo-based schiff bases ligands as highly active antifungal and antioxidant components, Heteroat. Chem. 2019 (2019).
[9] M.R. Grimmett, Imidazole and Benzimidazole Synthesis, Academic Press, 1997.
[10] N.O. Mahmoodi, S. Rahimi, M.P. Nadamani, Microwave-assisted synthesis and photochromic properties of new azo-imidazoles, Dyes Pigments 143 (2017) 387–392.
[11] E. Vitaku, D.T. Smith, J.T. Njardarson, Analysis of the structural diversity, substitution patterns, and frequency of nitrogen heterocycles among us FDA approved pharmaceuticals: miniperspective, J. Med. Chem. 57 (24) (2014) 10257–10274.
[12] P. Arora, V. Arora, H. Lamba, D. Wadhwa, Importance of heterocyclic chemistry: a review, Int. J. Pharmaceut. Sci. Res. 3 (9) (2012) 2947.
[13] L.D. Quin, J.A. Tyrell, Fundamentals of Heterocyclic Chemistry: Importance in Nature and in the Synthesis of Pharmaceuticals, John Wiley & Sons, 2010.
[14] S. Pramanik, S. Dhara, S.S. Bhattacharyya, P. Chattopadhyay, Separation and determination of some metal ions on new chelating resins containing N, N donor sets, Anal. Chim. Acta 556 (2) (2006) 430–437.
[15] M.A. Martins, C.P. Frizzo, D.N. Moreira, N. Zanatta, H.G. Bonacorso, Ionic liquids in heterocyclic synthesis, Chem. Rev. 108 (6) (2008) 2015–2050.
[16] J. Alvárez-Builla, J. Barluenga, Heterocyclic compounds: an introduction, Mod Heterocycl Chem 1 (2011) 1–9.
[17] K. Al-Adilee, H.A. Kyhoiesh, Preparation and identification of some metal complexes with new heterocyclic azo dye ligand 2-[2−-(1-Hydroxy-4-Chloro phenyl) azo]-imidazole and their spectral and thermal studies, J. Mol. Struct. 1137 (2017) 160–178.
[18] S. Shibata, M. Furukawa, R. Nakashima, Syntheses of azo dyes containing 4, 5-diphenylimidazole and their evaluation as analytical reagents, Anal. Chim. Acta 81 (1) (1976) 131–141.
[19] A.T. Henrici, The staining of yeasts by Gram's method, The Journal of medical research 30 (3) (1914) 409.
[20] X.-Y. Ni, H. Liu, L. Xin, Z.-B. Xu, Y.-H. Wang, L. Peng, et al., Disinfection performance and mechanism of the carbon fiber-based flow-through electrode system (FES) towards Gram-negative and Gram-positive bacteria, Electrochim. Acta (2020) 135993.
[21] M.A. Randhawa, Calculation of LD50 values from the method of Miller and Tainter, 1944, J. Ayub Med. Coll. Abbottabad 21 (3) (2009) 184–185.
[22] A. Al-Ali, A.A. Alkhawajah, M.A. Randhawa, N.A. Shaikh, Oral and intraperitoneal LD50 of thymoquinone, an active principle of Nigella sativa, in mice and rats, J. Ayub Med. Coll. Abbottabad 20 (2) (2008) 25–27.

[23] Arambašić MB, Randhawa MA, Arandjelović VM. Detailed Algorithms of Interactive Computer Programs in MATLAB for the Calculation of LD50 and Other LD Values Using Methods of Finney, Miller-Tainter and Comparison with OECD.
[24] W. Bartsch, G. Sponer, K. Dietmann, G. Fuchs, Acute toxicity of various solvents in the mouse and rat. LD50 of ethanol, diethylacetamide, dimethylformamide, dimethylsulfoxide, glycerine, N-methylpyrrolidone, polyethylene glycol 400, 1, 2-propanediol and Tween 20, Arzneim. Forsch. 26 (8) (1976) 1581–1583.
[25] J.S. Akhila, D. Shyamjith, M. Alwar, Acute toxicity studies and determination of median lethal dose, Curr. Sci. (2007) 917–920.
[26] B.B. de Menezes, L.M. Frescura, R. Duarte, M.A. Villetti, M.B. da Rosa, A critical examination of the DPPH method: Mistakes and inconsistencies in stoichiometry and IC50 determination by UV–Vis spectroscopy, Anal. Chim. Acta 1157 (2021) 338398.
[27] Andrzej L. Dawidowicz, Dorota Wianowska, Olszowy. Małgorzata, On practical problems in estimation of antioxidant activity of compounds by DPPH method (Problems in estimation of antioxidant activity), Food Chem. 131 (3) (2012) 1037–1043.
[28] Sk A. Islam, K. Kundu, P.K. Kundu, Azobenzene isomerization-induced photomodulation of electronic properties of N-heterocyclic carbenes, Chemistry–A European Journal (2020).
[29] K.J. Al-Adilee, K.A. Abedalrazaq, Z.M. Al-Hamdiny, Synthesis and spectroscopic properties of some transition metal complexes with new azo-dyes derived from Thiazole and imidazole, Asian J. Chem. 25 (18) (2013).
[30] L. Serrano-Andrés, M.P. Fülscher, B.O. Roos, M. Merchán, Theoretical study of the electronic spectrum of imidazole, J. Phys. Chem. 100 (16) (1996) 6484–6491.
[31] D.P. Drolet, D.M. Manuta, A.J. Lees, A. Katnani, G.J. Coyle, FT-IR and XPS study of copper (II) complexes of imidazole and benzimidazole, Inorg. Chim. Acta. 146 (2) (1988) 173–180.
[32] M. Al-Hussainawy, Kyhoiesh H. Synthesis, Spectral characterization and biological activity of 2-[2-(1-amino-1, 5-dinitrophenyl) azo]-imidazole, Journal of Global Pharma Technology 11 (7) (2019) 165–174.
[33] J. Torrens-Serra, I. Peral, J. Rodriguez-Viejo, M. Clavaguera-Mora, Microstructure evolution and grain size distribution in nanocrystalline FeNbBCu from synchrotron XRD and TEM analysis, J. Non-Cryst. Solids 358 (1) (2012) 107–113.
[34] H. Khan, A.S. Yerramilli, A. D'Oliveira, T.L. Alford, D.C. Boffito, G.S. Patience, Experimental methods in chemical engineering: X-ray diffraction spectroscopy—XRD, Can. J. Chem. Eng. 98 (6) (2020) 1255–1266.
[35] U. Holzwarth, N. Gibson, The Scherrer equation versus the'Debye-Scherrer equation, Nat. Nanotechnol. 6 (9) (2011) 534.
[36] G. Dini, R. Ueji, A. Najafizadeh, S. Monir-Vaghefi, Flow stress analysis of TWIP steel via the XRD measurement of dislocation density, Mater. Sci. Eng., A 527 (10-11) (2010) 2759–2763.
[37] R.B. Prime, H.E. Bair, S. Vyazovkin, P.K. Gallagher, A. Riga, Thermogravimetric Analysis (TGA). Thermal Analysis of Polymers: Fundamentals and Applications, 2009, pp. 241–317.
[38] A.A. Thamer, H.A. Yusr, N.J. Jubier, TGA, DSC, DTG properties of epoxy polymer nanocomposites by adding hexagonal boron nitride nanoparticles, J. Eng. Appl. Sci. 14 (2) (2019) 567–574.
[39] M. Khajehzadeh, M. Moghadam, S. Rahmaniasl, Structural, spectroscopic characterization (UV–vis, FT–IR and NMR) and TGA, TEM, FE–SEM, NBO and FMO analysis for (PdII–PNHC) n@ nSiO2, J. Mol. Struct. 1204 (2020) 127526.
[40] Zeinab Fereshteh, Masoud Salavati-Niasari, Effect of ligand on particle size and morphology of nanostructures synthesized by thermal decomposition of coordination compounds, Adv. Colloid Interface Sci. 243 (2017) 86–104.
[41] M. Salavati-Niasari, J. Javidi, F. Davar, A.A. Fazl, Sonochemical synthesis of Dy2 (CO3) 3 nanoparticles and their conversion to Dy2O3 and Dy (OH) 3: effects of synthesis parameters, J. Alloys Compd. 503 (2) (2010) 500–506.
[42] M. Salavati-Niasari, G. Hosseinzadeh, F. Davar, Synthesis of lanthanum hydroxide and lanthanum oxide nanoparticles by sonochemical method, J. Alloys Compd. 509 (10) (2011) 4098–4103.
[43] F. Davar, M. Salavati-Niasari, S. Baskoutas, Temperature controlled synthesis of SrCO3 nanorods via a facile solid-state decomposition rout starting from a novel inorganic precursor, Appl. Surf. Sci. 257 (9) (2011) 3872–3877. .
[44] H. Zhang, D. Yang, X. Ma, Y. Ji, S. Li, D. Que, Self-assembly of CdS: from nanoparticles to nanorods and arrayed nanorod bundles, Mater. Chem. Phys. 93 (1) (2005) 65–69.
[45] K. Thangavelu, K. Parameswari, K. Kuppusamy, Y. Haldorai, A simple and facile method to synthesize Co3O4 nanoparticles from metal benzoate dihydrazinate complex as a precursor, Mater. Lett. 65 (10) (2011) 1482–1484. .
[46] M. Creixell, A.P. Herrera, V. Ayala, M. Latorre-Esteves, M. Pérez-Torres, M. Torres-Lugo, C. Rinaldi, Preparation of epidermal growth factor (EGF) conjugated iron oxide nanoparticles and their internalization into colon cancer cells, J. Magn. Magn Mater. 322 (15) (2010) 2244–2250.
[47] B. Aslibeiki, P. Kameli, M.H. Ehsani, H. Salamati, G. Muscas, E. Agostinelli, D. Peddis, Solvothermal synthesis of MnFe2O4 nanoparticles: the role of polymer coating on morphology and magnetic properties, J. Magn. Magn Mater. 399 (2016) 236–244.
[48] S.K. Kyei, O. Akaranta, G. Darko, Synthesis, characterization and antimicrobial activity of peanut skin extract-azo-compounds, Scientific African (2020), e00406.
[49] M. Odabaşoğlu, Ç. Albayrak, R. Özkanca, F.Z. Aykan, P. Lonecke, Some polyhydroxy azo–azomethine derivatives of salicylaldehyde: synthesis, characterization, spectroscopic, molecular structure and antimicrobial activity studies, J. Mol. Struct. 840 (1-3) (2007) 71–89.
[50] S.B. Mohamed-Smati, F.L. Faraj, I. Becheker, H. Berredjem, F. Le Bideau, M. Hamdi, et al., Synthesis, characterization and antimicrobial activity of some new azo dyes derived from 4-hydroxy-6-methyl-2H-pyran-2-one and its dihydro derivative, Dyes Pigments (2020) 109073.
[51] S.A. Jaber, H.A. Kyhoiesh, S.H. Jawad, Synthesis, characterization and biological activity studies of cadmium (II) complex derived from azo ligand 2-[2\-(5-bromo Thiazolyl) azo]-5-dimethyl amino benzoic acid, in: InJournal of Physics: Conference Series, 1818, IOP Publishing, 2021 Mar 1, 012013. No. 1.
[52] L.C. Miller, M. Tainter, Estimation of the ED50 and its error by means of logarithmic-probit graph paper, Exp. Biol. Med. 57 (2) (1944) 261–264.
[53] A. Boente-Juncal, C. Vale, M. Camiña, J.M. Cifuentes, M.R. Vieytes, L.M. Botana, Reevaluation of the acute toxicity of palytoxin in mice: determination of lethal dose 50 (LD50) and No-observed-adverse-effect level (NOAEL), Toxicon 177 (2020) 16–24.
[54] M. Ghosh, Fundamental of Experimental Pharmacology Scientific, Book Agency, Calcutta India, 1984, p. 53.
[55] J. Lappi, J. Luoranen, Testing the differences of LT50, LD50, or ED50, Can. J. For. Res. 48 (6) (2018) 729–734.
[56] M.T. Tion, H. Fotina, S.A. Saganuwan, Phytochemical screening, proximate analysis, median lethal dose (LD50), hematological and biochemical effects of various extracts of Abrus precatorius seeds in Mus musculus, Journal of Advanced Veterinary and Animal Research 5 (3) (2018) 354–360.
[57] Linn Leaves, L. Leaves, Antioxidant activity by DPPH radical scavenging method of ageratum conyzoides, Am. J. Ethnomed. 1 (4) (2014) 244–249.
[58] Kitima Sirivibulkovit, Souksanh Nouanthavong, Yupaporn Sameenoi, Based DPPH assay for antioxidant activity analysis, Anal. Sci. 34 (7) (2018) 795–800.